Physica Scripta

PAPER

Ultrafast spin dynamics in magnetic trimer and tetramer clusters: a step towards prototypic spin-SHIFT registers

G Lefkidis[1,2], D Chaudhuri[3], W Jin[4], C Li[1], D Dutta[2] and W Hübner[2]

[1] School of Mechanics, Civil Engineering and Architecture, Northwestern Polytechnical University, Xi'an 710072, People's Republic of China
[2] Department of Physics, Rheinland-Pfälzische Technische Universität Kaiserslautern-Landau, PO Box 3049, 67653 Kaiserslautern, Germany
[3] School of Physics, Trinity College Dublin, Dublin 2, Ireland
[4] School of Physics and Information Technology, Shaanxi Normal University, Xi'an 710119, People's Republic of China

E-mail: lefkidis@rptu.de

Keywords: quantum information, quantum chemistry, magnetic logic, nanospintronics

OPEN ACCESS

RECEIVED
17 September 2023

REVISED
10 January 2024

ACCEPTED FOR PUBLICATION
22 January 2024

PUBLISHED
2 February 2024

Abstract

Ultrafast magnetic dynamics is a necessary ingredient for magnetic recording and ultrafast information processing. The shift functionality, although not mandatory for Boolean logic, is always implemented in CMOS CPUs and therefore must be also present in magnetic logic. In this respect, using *ab initio* calculations we show ultrafast spin dynamics in molecular clusters such as Co_3^+CO and Ni_4. In this work, we establish that clusters with magnetic atoms can provide a theoretical toolbox for efficient spin charge dynamics whose operation time can range up to a few picoseconds. The prime underlying mechanism for all spin manipulation scenarios in the above mentioned clusters are laser-induced Λ processes where the laser parameters are fully optimized using a genetic algorithm. In general, a structural asymmetry enforces substantial spin localization on the active centers of both magnetic clusters. Keeping in mind the shift functionality, we theoretically suggest a series of spin-transfer scenarios between the Co and Ni atoms in each of these two clusters independently to construct a 3-bit and a 4-bit cyclic spin-SHIFT register, respectively. The maximum operational time for both logic devices is 2 ps, which is much faster than the response time of conventional spintronic devices. Additionally, for a better understanding of the transfer cycles, their feasibility and reversibility are also investigated through the analysis of the optical spectra of the related states. Our results provide important theoretical guidance for ultrafast spin manipulation in molecular structures as well as their potential spin functionality, and thus step closer to the realization of future spin-based logic devices and quantum computation. This effectively motivates the investigation and precise establishment of the shift functionality in magnetic trimers and tetramers.

1. Introduction

Since the past decade *spintronics* has created a buzz in the scientific arena. Contrary to the operations in conventional semiconductor technology, spin based operations can be utilized both in classical as well as in quantum computation at very small spatial and temporal scales. One aspect of this research is downscaling devices if possible down to the atomic scale [1–6], by harnessing the spin degree of freedom as information bit in Boolean logic [7–10].

Many theoretical studies have already shown the possibility of using light to induce ultrafast magnetic dynamics in extended systems [11, 12]. The spin magnetic moment improves reading/writing operations and can be used in more efficient data saving devices as magnetic random-access-memory (MRAM) [13–15]. The NOR and OR gates have been built by making use of the spin frustration and indirect exchange coupling [16]. Other than magnetic fields and electric currents, laser pulses have been proved to be effective tools to regulate and manipulate material spins [17]. Ultrafast laser pulses also probe the exchange interactions (0.01 ps to 0.1 ps time scale). The optical control of magnetic order has been thoroughly researched [18, 19]. A detailed review of the experimental state-of-the-art of molecular spintronics, as obtained with molecular magnetic materials can

be found, among others, in [20], and a road-map of single-molecule computing in [21]. If one can order and regulate molecular spins with ultrafast laser pulses, it would lead to enhancement of information storage density as well as information processing speed. Typical paradigms, such as molecular switches [22], single molecular magnets [23], atomic spin logic gates [4, 7, 24], and spin shift register in an atomic chains [25, 26] have been proposed and reported for future spin-based technological specialized applications.

Electronic circuits, which rely on magnetic molecules or clusters to perform Boolean logic have three advantages. Firstly, they require a minimum surface area to implement. Secondly, manipulating the spin degree of freedom the information transfer speed can be enhanced, and thirdly, such operations can be made non-volatile. In general, a sequential logic operation in a SHIFT register takes place in the form of storing and transferring information as binary data (0 and 1). This creates as a cascade of flip flops which loads the input data and shifts them after every clock pulse. Baskin *et al* emphasized the use of a molecular shift register as an autonomous DNA synthesizer [27]. Lengwenus *et al* reported the transport of 2D arrays of neutral atoms in a SHIFT like architecture [28]. This motivates the investigation of laser-driven ultrafast spin-based magnetic logic in multicenter magnetic clusters that exploits small momentum transfer, elementary excitations with significant energy differences and operates on a femtosecond time scale. In the present study we take a step ahead towards the development of prototypic 3-bit and 4-bit cyclic spin-shift registers with Co_3^+CO and Ni_4 magnetic clusters. We use third-row-transition metal as our preferred magnetic atoms primarily because they act as simple prototypic model systems which can easily be manipulated in experiments (mass spectrometry) and are less atomistic than the fourth-row-transition-metal atoms (in the sense that there is usually a larger overlap of their electronic states). Various properties of Co and Ni clusters have already been investigated [29–36], revealing that their complex electronic structure renders the optical manipulation of the spin very flexible and efficient.

The problem we need to address is how to design logic elements and storage devices for classical or even quantum computation, that are both effective and experimentally feasible. Recent progress in on-chip laser technology makes our design realistic [37–40]. In this study we investigate two magnetic clusters (namely Co_3^+CO and Ni_4) and show how they can be used for performing logic operations at the molecular level with operational times below 2 ps. Our focus turns to the pursuit for the spin transfer cycle involving all magnetic centers for each structure and the attempt to offer clear-cut theoretical trimer/tetramer toolboxes for spin-charge shift functionalities, which lie at the core of integrating logic elements in larger circuits.

The article is organized as following: In section 2 we present the *ab initio* theory and computational details pertaining to both the trinuclear and tetranuclear clusters. The electronic structure, optical spectra and ultrafast spin dynamics of Co_3^+CO and Ni_4 are presented in section 3.1 and section 3.2 respectively. Lastly, in section 4 we summarize of our findings.

2. Theory and computational details

Differently from other standard DFT-based approaches [41–44], we use highest-level quantum chemistry to study laser-induced ultrafast spin dynamics in molecular systems. In our calculations we treat the magnetic systems quantum mechanically in order to take into account the crucial effects of the static and dynamic correlations on the level of first-principles theory [10, 45]. Since the laser-matter interaction is steered by the electric-dipole transition matrix elements, calculating the many-body excited states and the wave functions accurately is a prerequisite. This eventually serves as a basis for our ultra-fast spin dynamics. The computations pertaining to the theory are performed in four steps as following:

(i) In the first step we solve the non-relativistic model Hamiltonian of the magnetic system without any external fields. The Hamiltonian reads

$$\hat{H}^{(0)} = -\frac{1}{2}\sum_{i=1}^{N_{\rm el}}\nabla^2 - \sum_{i=1}^{N_{\rm el}}\sum_{a=1}^{N_{\rm at}}\frac{Z_a}{|\mathrm{R}_a - r_i|} + \sum_{i=1}^{N_{\rm el}}\sum_{j=1}^{N_{\rm el}}\frac{1}{|r_i - \mathrm{r}_j|} + \sum_{a=1}^{N_{\rm at}}\sum_{b=1}^{N_{\rm at}}\frac{Z_a Z_b}{|\mathrm{R}_a - \mathrm{R}_b|}, \quad (1)$$

where $N_{\rm el}$ and $N_{\rm el}$ refer to the number of electrons and atoms, r_i and r_j refer to the position vectors of the electrons, R_a and R_b refer to the position vectors of the nuclei, and Z_a and Z_b are the charges of the nuclei. The third term in the right hand side of the equation is of maximum importance as it gives rise to the correlations. For example, the magnetic cluster shown in figure 1(a) is optimized at the Hartree–Fock (HF) level with the 6-31G(d) basis set [46, 47].

(ii) We perform the non-relativistic high-level quantum-chemistry calculations with the symmetry-adapted-cluster configuration-interaction (SAC-CI) method [48] since it is size consistent [49–52] and describes the

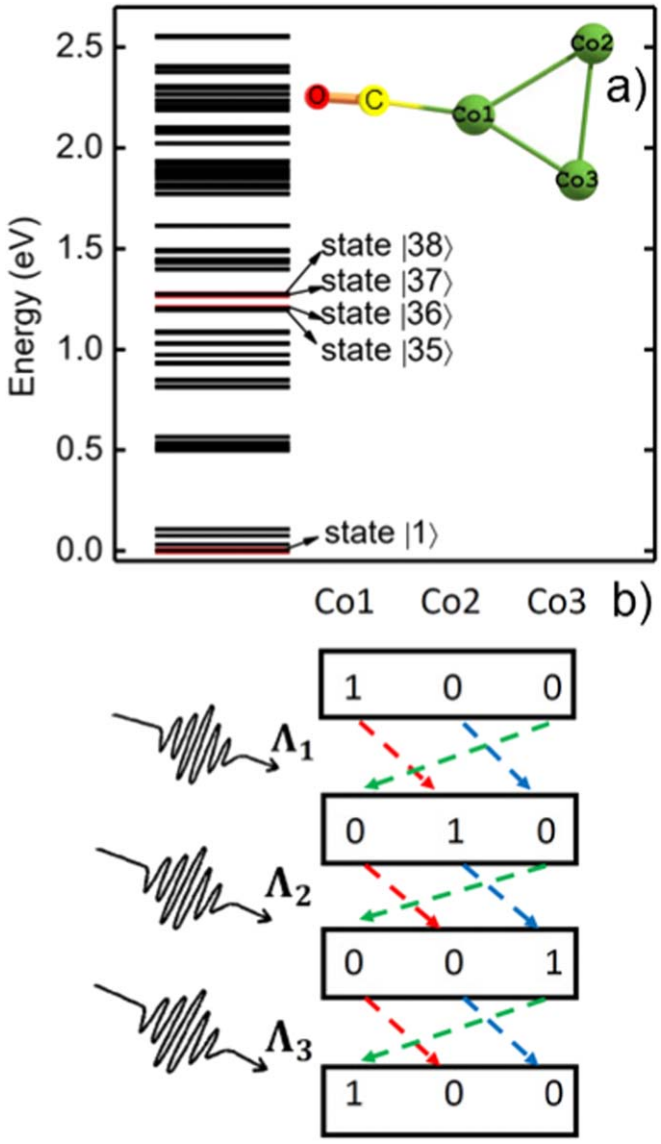

Figure 1. (a) The geometry of cluster Co_3^+CO and its energy levels obtained from SAC-CI method, among which the initial and final states ($|1\rangle$, $|35\rangle$ and $|37\rangle$) of the spin dynamics to be discussed below are marked here. Note, $|36\rangle$ and $|38\rangle$ are the spin mixed intermediate states for the processes. The applied **B** field is 2.35 T. (b) Illustration of the cyclic SHIFT register sequences in the cluster Co_3^+CO. The dashed arrows show the shift directions of the three bits.

$d-d$ and charge transitions accurately [45]. With this method it is possible to calculate a multitude of determinants that describe the correlations accurately [53]. Note that, during this the two kinds of electronic excitations that are taken into account are (a) virtual excitations from the single-determinantal reference state describe the many body nature of the state, and (b) real optical (laser) transitions between the many body states obtained in this way, which are mediated by dipole transition-matrix elements. The SAC-CI choice cost us less computational overhead, because, unlike multireference methods, it deals with only one orthogonal set of molecular orbitals. This allows us to take full advantage of the Slater-Condon rules. It is known that the presence of more determinants accounts for the correlational effects resulting in high-fidelity spin-dynamics scenarios. This further justifies the use of SAC-CI method because the many-body states of our systems typically consists of more than 1500 determinants.

(iii) Relativistic effects are taken into account by including the effect of spin–orbit coupling (SOC) and an external magnetic field ($\mathbf{B}_{\text{stat}}$). The corresponding time-independent Hamiltonian can be expressed as:

$$\hat{H}^{(1)} = \sum_{i=1}^{N_{\text{el}}} \frac{Z_a^{\text{eff}}}{2c^2 R_i^3} \hat{\mathrm{L}}_i \cdot \hat{\mathrm{S}} + \sum_{i=1}^{N_{\text{el}}} \mu_L \hat{\mathrm{L}}_i \cdot \mathrm{B}_{\text{stat}} + \sum_{i=1}^{N_{\text{el}}} \mu_S \hat{S}_i \cdot B_{\text{stat}} \tag{2}$$

For the results shown in this article, the applied B_{stat} is 2.35 T. With the use of the one-electron Breit operator the SOC is calculated. $\hat{L}$ and $\hat{S}$ are the orbital and spin angular momentum operators, μ_L and μ_S are their respective gyromagnetic ratios and c is the speed of light. Relativistic effective nuclear charges Z_a^{eff} are used to account for the two-electron integrals of SOC [54]. All terms used in equation (5) describe intrinsic properties of the material. The necessity for the Zeeman-splitting (second and third term in the above equation) arises among others from the need to (numerically) distinguish the different substates (different values of m_s) of the triplet states. Additionally it further lowers the symmetry of the system, thus creating more spin-mixed states, which can be used as intermediate states for our Λ processes. Thus, the total Hamiltonian after the inclusion of SOC and magnetic field is $\hat{H}^{\text{tot}} = \hat{H}^{(0)} + \hat{H}^{(1)}$. The eigenfunctions of the new Hamiltonian are expressed in terms of a linear combination of the eigenfunctions of the non-relativistic Hamiltonian i.e., $\hat{H}^{(0)}$. This is known as spin mixing.

(iv) To simulate the laser-matter interaction we take into account the effect of a tailored sech^2 shaped laser pulse. The time-dependent Hamiltonian is given as:

$$\hat{H}^{(2)}(t) = \hat{D} \cdot E_{laser}(t) \tag{3}$$

where $E_{tab2laser}(t)$ is the time-dependent electric field of the laser pulse, respectively, and $\hat{D}$ is the electric-dipole transition operator. The laser pulse is characterized by six key parameters, i.e., three angles (θ, ϕ, γ) associated with the direction, energy (E_ω), pulse duration **FWHM**, and amplitude. The magnetic-dipole interaction terms $\sum_{i=1}^{N_{el}} \mu_L \hat{L}_i \cdot B_{laser}(t)$ and $\sum_{i=1}^{N_{el}} \mu_S \hat{S}_i \cdot B_{laser}(t)$ are neglected in the calculation since they are usually about two orders smaller than the electric-dipole interaction.

Under the influence of it, the evolution of the system is described by the following coupled differential equations

$$i\hbar \frac{\partial}{\partial t} c_n(t) = \sum_k \langle \Phi_n | \hat{H}(t) | \Phi_k \rangle \, e^{\frac{i}{\hbar}(E_n - E_k)\cdot t} c_k(t), \tag{4}$$

and solved using a fifth-order Runge-Kutta method and the Cash-Karp adaptive-step control [55]. Here, $\hat{H}(t) = \hat{H}^{\text{tot}} + \hat{H}^{(2)}(t)$. E_n and E_k are the energies of state $|\Phi_n\rangle$ and $|\Phi_k\rangle$, respectively, and $c_k(t)$ is a time-dependent coefficient of the state $|\Phi_k\rangle$ in the total wave function $\Psi(t) = \sum_k c_k(t)|\Phi_k\rangle$. Driven by the well-tailored laser pulses and by choosing the appropriate initial and target states with different magnetic properties, certain spin functionalities can be achieved based on Λ processes through the participation of several spin-mixed intermediate states.

The laser-parameters are optimized using a specially designed genetic algorithm that searches for the most efficient paths to transfer the electronic population within the many-body Hilbert space with a high-fidelity yield [56]. The whole process takes place with the emission and absorption of a photon. Further computational details are given elsewhere [29–31, 45, 56, 57].

Ni_4 has been previously investigated using the augmented bi-linear biquadratic Heisenberg-Dirac-van-Vleck model spin-Hamiltonian [10]. These results differ substantially from the current full *ab initio* approach, since the model Hamiltonian, unlike the present calculation, does not correctly take into account electronic correlations. The model-spin Hamiltonian approach assumes that the exchange integrals have the same values for all electronic states regardless of their spatial composition.

3. Results

The results shown here assume that the clusters exist in gas phase. Thus, a generic question persists about the applicability of spin information storage in the gas phase. However, it has been shown that small molecules can be stable on surfaces [58–61]. The Fe_4 molecule retains most of its static and dynamic magnetic features when brought in a surface-vacuum layer [62]. The presence of a substrate does not cause change in the optical selection rules (the resonance might get slightly shifted though) in a molecule and the basic physics remains more or less unaltered [63, 64]. The purpose of this work is to establish prototypic spin-shift register functionalities. In this respect magnetic trimer and tetramer cluster serve as promising candidates. In simple terms it is a classical logic circuit that can store and transfer information through a sequential logic operator in the form of binary data and the flip flops share the same clock. Logic operations in such devices include a 'data in' and a 'data out' bit. The entire process is a destructive readout of operations since after each clock pulse (laser pulse in this case) the 'data out' bit is shifted out of the right most bit of the data string. However, such destructive operations can be essentially bypassed if the data string is cyclic in nature. A pictorial representation of such operation are shown in figure 1(b) where the magnetic atoms showing strong spin localization behavior are considered as the high (1) and low (0) data types otherwise. The respective localization for Co1, Co2 and Co3 are $|37\rangle$, $|1\rangle$ and $|35\rangle$

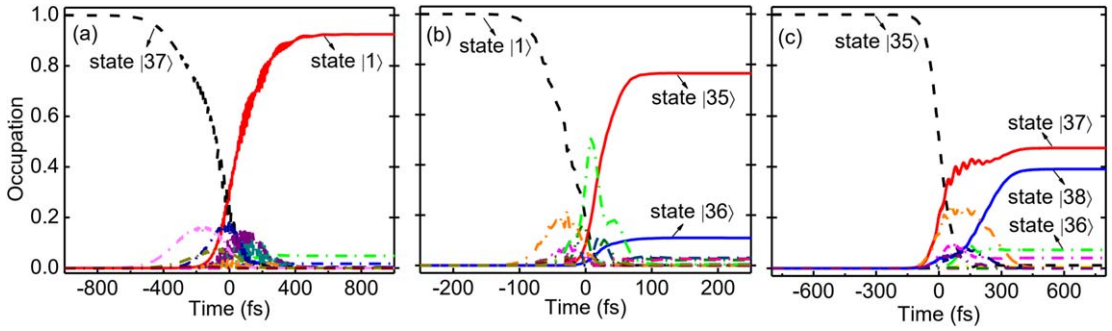

Figure 2. (a), (b) and (c) are the time-resolved occupations for spin-transfer scenarios of Co1 → Co2 (process Λ_1), Co2 → Co3 (process Λ_2) and Co3 → Co1 (process Λ_3) in Co_3^+CO, respectively, in which the corresponding initial (dashed) and final (solid) states for each scenario are marked. The evolution of the intermediate states in each scenario are denoted by the dash-dotted lines.

respectively. A more detailed description of the states participating in the transfer operations are given below. In principle at every given point of time all bits can be read out and no data is lost and the laser pulse replaces the conventional clock. This motivates essentially the quest for closed chain tri(tetra)-nuclear clusters. Therefore it remains within the reach of our effort to realize the technology using molecular spins.

3.1. Co_3^+CO

The electronic properties and magnetic dynamical behavior are structure dependent. Thus, one can assume that for the same magnetic trimer, a different ligand can yield distinct spin scenarios (here it refers to spin transfer) with properly-distributed spin states. To verify it, in this article we attach a popular marker molecule, i.e., CO, to Co_3^+ with the expectation of getting spin transfer scenarios between the magentic centers (see figure 1(a)). From previous calculations we know that it is important to maintain a delicate balance between too high symmetry (which disallows spin localization) and too low symmetry (which completely closes the paths between the states with different spin localization: the magnetic atoms behave more as isolated) [32, 45].

Pure Co_3^+ molecules are extremely symmetric and thus the spin fails to localize on the magnetic centers. On the other hand, attaching other ligands such as CH_3OH and C_2H_5OH lowers the overall symmetry but all spin dynamics scenarios are only restricted to spin switching [32, 65]. The attachement of the larger ligands induces a higher degree of distortion of the Co_3^+ segment and as a result exerts a negative effect on the transitions between the electronic states with different spin localizations (e.g., the transitions are either allowed but with very low fidelity or totally forbidden). In this respect the carbonyl ligand (CO) appears to be a good alternative for the following four reasons (i) it serves as a good experimental marker to monitor different magnetic states through its vibrational frequency analysis [66], (ii) it has wide-spread applications in the reaction of gas phase transition metals due to its reactivity properties [67], (iii) it lowers the local symmetry of highly symmetric bare clusters resulting in substantial localization of spins on the active centers and allowing us to investigate local spin manipulation scenarios, and (iv) we have previously successfully studied the laser-induced ultrafast molecular rotational dynamics for the application of a molecular rotatory motor [68].

3.1.1. Spin dynamics and optical spectra

The most-stable geometry of Co_3^+CO [68] and its 120 low-lying triplet states are obtained by the symmetry-adapted-cluster configuration interaction (SAC-CI) method [48]. The energy levels of the electronic excited states after the inclusion of SOC and an external magnetic field are shown in figure 1(a), in which the positions of the initial, main intermediate, and final states of the three spin-dynamics scenarios to be discussed below are marked. By searching the addressable channels for which the initial and final states have different spin localizations in the energy region of 0−2eV, three transfer scenarios Λ_1, Λ_2 and Λ_3, i.e., $|37\rangle \rightarrow |1\rangle$ (92%), $|1\rangle \rightarrow |35\rangle$ (76%) / 36 (11%), and $|35\rangle \rightarrow |37\rangle$ (47%) / 38 (39%), are found, as shown in figure 2. Here, in each dynamics only the individuals with noticeable final occupations (denoted by the percentage numbers in the parentheses) are considered. Table 1 lists the energies, spin expectation values, and spin densities of the initial and final states in the three scenarios. Note that in this article the notions 'spin localization' and 'spin orientation' refer to the overall spin density localization and the relative magnitudes of the quantum mechanical spin operators. It is important to keep in mind that although spin is not a good quantum number in the presence of SOC, it is still meaningful if the spin expectation values of the initial and final states, which are chosen near the ground state, are relatively large (which means that they are close to the pure spin states without SOC). It is not possible to calculate the exact spin values (S^2 and S_z) of the new states (after SOC). However, quantum mechanical expectation values of the spins can always be calculated.

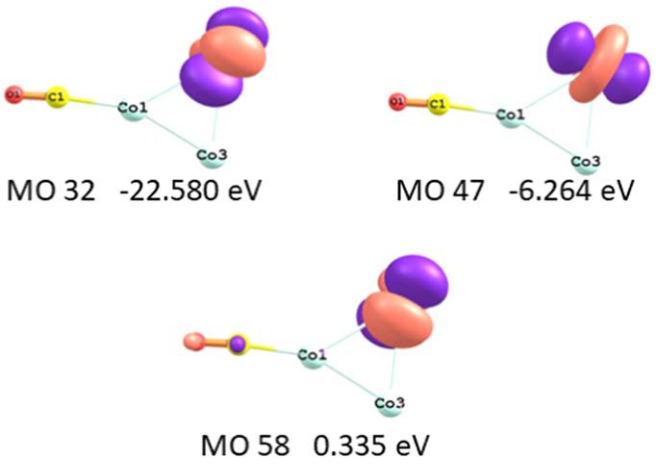

Figure 3. Some of the strongly localized, single electron, *d*-character molecular orbitals for Co2 in the Co_3^+CO cluster. The multiplicity of the cluster for the HF step is a triplet. The isosurfaces of the molecular orbitals are dark violet and orange for positive and negative values, respectively.

Table 1. Energies, spin expectation values, and spin densities of the initial and final states of Co_3^+CO in the spin-transfer scenarios discussed in this manuscript.

State	Energy (eV)	$\langle S_x \rangle$	$\langle S_y \rangle$	$\langle S_z \rangle$	$\langle S \rangle$	Spin density		
						Co1	Co2	Co3
37	1.272	−0.037	−0.008	0.464	0.465	1.225	0.513	0.268
35	1.205	−0.556	−0.520	0.048	0.763	0.074	0.018	1.906
1	0.000	−0.255	−0.188	−0.012	0.318	0.014	1.982	−0.009

From the values of spin densities one can clearly see that the spin localization of $|1\rangle$, $|35\rangle$ and $|37\rangle$ is on Co2, Co3, and Co1 (see table 1), respectively. As an example figure 3 shows some of the most important *d*-character molecular orbitals (MO) resulting from the HF calculation that are localized on Co2. Note that the high-correlated post-HF wave functions cannot be described with such simple pictures but they still serve the purpose of tracing out the main virtual one-electron excitations. These give a first-hand insight into the spin localization of the different many-body electronic states discussed in the spin transfer scenarios. For $|1\rangle$ the the dominant excitations are from MO 47 (d_y^2) → MO 58 (d_{xz}) with a coefficient of 0.75 and MO 32 ($d_{x^2-z^2}$) → MO 58 (d_{xz}) with a coefficient of −0.61, respectively.

Since the main final individual states in each scenario stem from the same triplet term before the inclusion of SOC (and the magnetic field) and have the same spin localization, a cycle of spin transfer, that is Co1 → Co2 → Co3 → Co1, is thus achieved. The fidelity of each dynamics scenario is 92%, 85%, and 93%, respectively, which therefore contributes to a total efficiency of 73%. It should be noted that here the fidelity of the latter two scenarios (the final states of which are quantum superpositions of two main individual states) is redefined as $\frac{1}{\sqrt{2}}(\sqrt{p_1} + \sqrt{p_2})$, where p_1 and p_2 are the final occupations of the two individual states. For the implementation, after obtaining the third transfer process Λ_3 which ends at two individual states with almost equal probabilities, one can always choose state $|37\rangle$ (even if the systems ends at state $|38\rangle$, since a spin-flip scenario can easily solve this problem) as the initial state to restart and accomplish the whole cycle. The optimized parameters of the laser pulses for the three transfer processes are given in table 2. Among the three scenarios, the second one [Λ_2, as shown in figure 2(b)] turns out to be the fastest with respect to the FWHM as well as the time duration of the whole process.

In order to seek the possibility of gaining an additional path to extend the functionality, the whole transfer cycle in an anticlockwise direction (i.e., Co1 → Co3 → Co2 → Co1) is also investigated. It is sought for, by exchanging the initial and final states of each scenario in two different ways: one is to try the reverse process by keeping the same laser parameters as the previously achieved one, and the other is to search for a new reverse process without any laser parameter confinement or reference. It turns out that the opposite cycle is blocked due to the unachievable spin transfer process from $|35\rangle$ to state $|1\rangle$. Specifically, in the first case the system mainly ends at a superposition of $|35\rangle$ (28%), $|36\rangle$ (10%), $|118\rangle$ (39%, spin localization Co1), and $|120\rangle$ (13%, spin localization Co1), and in the latter way no addressable transfer scenario has been found using the genetic

Table 2. The optimized parameters of the laser pulses for the spin-transfer scenarios in Co_3^+CO discussed in this manuscript. Here, θ and ϕ denote the angles of the incidence in spherical coordinates, and γ is the angle between the polarization of the light and the optical plane. FWHM is the full width at half maximum of the laser pulse.

Transfer process	$\theta(^\circ)$	$\phi(^\circ)$	$\gamma(^\circ)$	Intensity(J s^{-1} m^{-2})	FWHM(fs)	Energy(eV)
Λ_1 (Co1 → Co2)	38.7	159.4	327.0	0.26	503	1.30
Λ_2 (Co2 → Co3)	53.5	22.2	245.6	0.20	95	1.32
Λ_3 (Co3 → Co1)	46.8	286.1	230.1	0.20	299	1.25

algorithm. To understand the irreversibility of process Λ_2, a detailed inspection into the dynamics in figure 2(b) is performed. It shows that there are 23 intermediate states involved [which is three and 12 states more than that in scenarios Λ_1 and Λ_3, respectively], and among them several states have noticeable occupations during the propagation. This makes the evolution of whole process complicated and brings about the difficulty for the system going backwardly to the desired initial state, especially for the case when the fidelity of the final state is relatively low [69]. As expected, it is found that the intermediate state with the largest occupation [denoted with the grey dash-dotted line in figure 2(b)] is just $|118\rangle$, and thus explains why the system goes to this state largely in the reverse process mentioned in the first trial. For the other two reverse transfer processes performed in the same way, the final states end up with 37% on $|37\rangle$ and 15% on state $|38\rangle$ for process Λ_1^* ($|1\rangle \rightarrow |37\rangle$), and 86% on $|35\rangle$ for process Λ_3^* ($|37\rangle \rightarrow |35\rangle$), respectively. Here, the low reversibility of Λ_1 is due to the involvement of too many intermediate states, and the high reversibility of Λ_3 is quite understandable since the initial and final states are very close to each other (more balanced for both of the transfer directions) and only 11 intermediate states are involved (less interference when propagating). The new reverse processes of these two scenarios with efficiencies 64% and 82% are also achieved using the second way, which are not shown here since no new features are exhibited. The reader should keep in mind, that the irreversibility mentioned here does not rely on the breaking of the time-symmetry of the Hamiltonian [70], but on the loss of quantum coherences and the pertinent lowering of the information entropy of the system [57].

3.1.2. Application: 3-bit SHIFT register

Before delving into the discussion of the trimer's application as a shift-register it is important to discuss the lifetime of the states. In general the lifetime of the states must be longer than the maximum operation time required for the magnetic logic [7]. According to the DiVincenzo critieria a 'fault-tolerant' error correction is possible if the decoherence time is four orders of magnitude longer than the clock time [71]. Thus, the choice of our molecular systems for spin logic operations are clearly in advantage due to the absence of conformational changes [72]. For example spin relaxation times for heterometallic wheels such as the $Cr_7Ni(Mn)$ is of the order of microseconds [73]. Previously, our theoretical studies on a tri-nuclear Ni cluster (Ni_3Na_2) showed that the longitudinal relaxation time T_1 and transverse relaxation time T_2 are calculated to be about 10 times slower if they are mediated through phonons than through laser pulses [74].

For application, the cycle of spin transfers shown in figures 2(a), (b) and c) can be used as a simple cyclic SHIFT register or a ring counter [75]. The mechanism is illustrated as following [as shown in figure 1(b)]: for the initial spin localization configuration $|100\rangle$ (denotes that the spin localizes on Co1) in the atomic order of Co1 Co2 Co3, after the three hop operations $|100\rangle \xrightarrow{\Lambda_1} |010\rangle \xrightarrow{\Lambda_2} |001\rangle \xrightarrow{\Lambda_3} |100\rangle$ the three-bit state goes back to the original configuration accompanied by three kinds of shiftings. Here, we define the atom with spin localized as bit 1 (otherwise 0) and consider the transfer process driven by proper laser pulses as a trigger to shift the spin. Note that for each operation, the first two bits in the previous state are shifted together to the right by one step while the last bit becomes the first bit of the next state. The whole operation time completes within around 2 ps, which is fast compared to the response of conventional charge-based logical devices. Different from the spin SHIFT register proposed in Ref. [25], which transports spin information by moving an electron down a one-dimensional chain of N identical atoms (which each have a spin state of $S = 1/2$), the pure spin-based functionality in this article shifts the spin from one spin-localized site to the other through coherent laser-induced ultrafast spin transfer processes. Despite of its conceptual simplicity and functional limitation, this is quite promising for future quantum information processing and is believed to be practical possible with the development of spin-detecting and -controlling techniques.

3.2. Ni_4

Ni_4 clusters have been an interesting subject for investigations in the recent past. Kirchner *et al* showed that the antisymmetric exchange interaction is a result of the mixing of the pseudoangular momentum and the ground state spin multiplet [76]. The stability, electronic and magnetic properties of various symmetries (of Ni_4) have been studied with DFT based methods in presence of impurity atoms [77]. In general the structural aspects of

realistic magnetic systems with few magnetic atoms which give rise to magnetic nanologic have been studied thoroughly. In this respect, the role of correlations, the number of active centers, the geometry (linear vs bent molecules, triangles, fullerenes, planar and nonplanar geometries) [78, 79], and of attached ligands (CO, ethanol, methanol, etc.) have been studied extensively. In the following section we explore the functionalities arising from using a model system with four rather than three magnetic centers and develop a protypic 4-bit SHIFT register with it and exploiting spins as the only information carriers.

In quest for a Toffoli like gate where the input information is not lost even after the logic operation, Ni_4 is good candidates as it fulfills the minimum of centers required for such a magentic logic operation where one atom can be used as an auxiliary bit while the rest three can be used as input and output bits. Other than that the exclusive dependence of magnetic field as input carrier can be bypassed with four centers. The disparate nature of the interatomic distanctes facilitates the localization of the spins on the magnetic centers. In the past we have elaborately demonstrated the importance of electronic excitations for magnetic interaction in Ni_4 and successfully established a pure-spin OR gate with the same. In addition to a 3-bit cyclic SHIFT register with the Co_3^+CO cluster, we also go one-step further and propose a 4-bit quantum-spin-SHIFT register based on the spin transfer scenarios between the inter-atomic centers of Ni_4 with different bond lengths. Furthermore, we also give a plausible suggestion to implement such read and write operations on our molecular clusters.

3.2.1. Spin dynamics

To demonstrate an all-spin SHIFT register we choose a planar Ni_4 cluster as our model system as shown in figure 5(a) (right panel). Depending on the environment it can exist in two other forms such as a) chain [80], and b) a tetrahedral structure mainly [76]. For technological applications it is important to consider not only the geometry of a bare cluster in the vacuum but also a physical situation. Thus we assume the most probable conformation of the cluster when deposited on a surface, namely a two dimensional one. Surface deposition is an appropriate way to tackle the challenge of the molecular orientation and geometrical stability at room temperature (in the gas phase). Note that we want to demonstrate the proof-of-principles for the suggested functionality. Therefore, the following model system consists of the minimum ingredients necessary, namely a flat molecule with disparate inter-atomic distances and spin–orbit coupling for the spin dynamics, hence the choice of a bare planar structure [see figure 4(a)]. The planar Ni_4 is optimized at the HF level with the Los Alamos basis set (LANL2DZ) and scalar relativistic effective core potentials (Ni[8s5p5d/3s3p2d]) [81, 82]. The ground and 100 excited states (30 triplets and 10 singlets) are calculated using the SAC-CI method [48]. Most of the spin transfer scenarios and the pertinent initial and final states for the processes have been already discussed previously [10]. It is particularly important to recapitulate the spin dynamics scenarios as the prototypic spin-shift register with the Ni_4 cluster stem from these. All details with respect to the spin transfer scenarios namely the energy of the states, the spin expectation values (S_x, S_y, S_z,) and the spin density distribution information are summarized in table 3. Once the information of the states involved for the spin transfer scenarios between atoms Ni1, Ni2, Ni4 and Ni3 are obtained, a pictorial representation of the prototypic shift register is proposed in figure 4(b). It is evident that after the influence of every laser pulse (Λ_1, Λ_2, Λ_3 and Λ_4) the 'data out' bit is shifted out of the right most bit of the data string. A detailed description of the mechanism is presented in section 3.2.2. The corresponding laser optimized parameters are shown in table 4. Additionally, we report a new spin transfer scenario $|16\rangle \rightarrow |25\rangle$ (Ni3 → Ni1) that ends within 400 fs with a fidelity of 91%. This is essentially the penultimate transfer scenario for the functionalization of the 4-bit cyclic shift register. From the spin density information given in table 3 it clear that for $|25\rangle$ the spin is localized mainly on Ni1. Figure 5(a) refers to the transfer of the population between the initial state ($|16\rangle$, marked with solid black line) and final state ($|25\rangle$, marked with dashed-red line) via the three intermediate states $|3\rangle$, $|14\rangle$ and $|15\rangle$. The respective energies of the initial and final state are $E_{|16\rangle} = 0.984$ eV and $E_{|25\rangle} = 1.380$ eV.

Note, the $|14\rangle \rightarrow |16\rangle$ (Ni4 → Ni3) spin transfer process has been recalculated and reported here with a higher fidelity of 80% (after the inclusion of SOC). Accordingly, the pertinent laser pulse resulting in transferring the population from $|14\rangle$ to $|16\rangle$ has been re-optimized and the new set of parameters are $\theta = 26.56°$, $\phi = 210.27°$, $\gamma = 188.13°$, $FWHM = 330.19$ fs, and $E_\omega = 0.06$ eV (see table 4). As an example in figure 6 for the many body state $|14\rangle$ we show the major one-electron virtual excitation from MO 26 (strong $d_{x^2-y^2}$ character localized on Ni4) to MO 51 (strong d_z^2 character localized on Ni4) with a CI coefficient of 0.665. Similarly, for the many body state $|16\rangle$ one of the major one electron virtual excitation takes place from MO 31 (strongd_y^2 character localized on Ni3) to MO 51 (partially strong d_x^2 character localized on Ni3) with a CI coefficient of 0.406.

Figure 5(b) corresponds to the expectation values of the spin angular momentum components namely $\langle S_x \rangle$, $\langle S_y \rangle$ and $\langle S_z \rangle$. The magnitude of the applied magnetic field **B** is 2.35 T along the z axis of the molecule. Thus, we see that the $\langle S_z \rangle$ gets affected the most. The transient occupations of the intermediate states are 37%, 68% and 23% approximately. Lastly the envelope of the laser pulse is given in figure 5(c) and the corresponding optimized laser parameters are $\theta = 100.86°$, $\phi = 15.84°$, $\gamma = 275.01°$, $FWHM = 421.69$ fs, and $E_\omega = 3.15$ eV (see table 4).

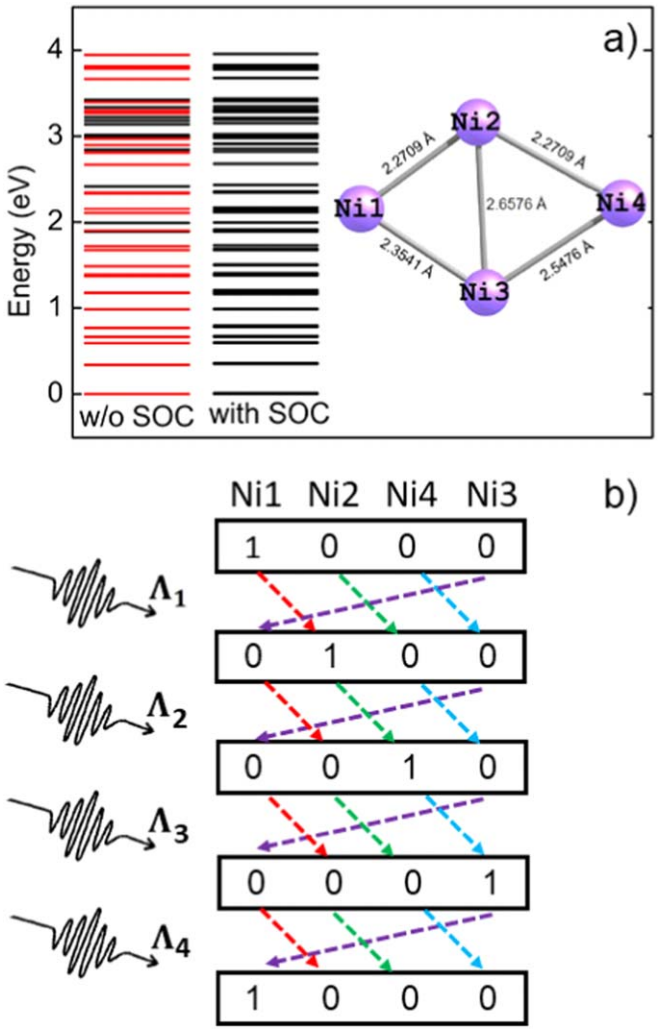

Figure 4. (a) Electronic excited states of the optimized Ni_4 as calculated with the SAC-CI method for states up to 4 eV. Left: without spin–orbit coupling, singlet states are given with the solid black lines, triplet states with the red lines, Middle: after the inclusion of spin–orbit coupling (there can be no distinction between singlets and triplets after spin–orbit coupling), Right: Optimized structure of planar Ni_4 at the Hartree–Fock level (details in [10]). The applied **B** field is 2.35 T. (b) Illustration of the cyclic SHIFT register sequences in the Ni_4 cluster. The dashed arrows show the shift directions of the four bits.

Table 3. Energies, spin expectation values, and spin densities of the initial and final states of Ni_4 in the spin-transfer scenarios discussed in this manuscript.

State	Energy (eV)	$\langle S_x \rangle$	$\langle S_y \rangle$	$\langle S_z \rangle$	$\langle S \rangle$	Spin density			
						Ni1	Ni2	Ni3	Ni4
14	0.79	0.33	0.00	0.41	0.526	0.032	0.307	0.685	2.541
16	0.98	0.39	0.00	−0.41	0.565	0.184	0.321	2.168	0.635
25	1.37	−0.44	0.01	0.24	0.501	1.248	1.119	0.999	0.283
51	2.34	−0.76	0.00	−0.21	0.788	0.895	0.282	0.083	0.322
54	2.35	−0.76	0.00	−0.04	0.761	0.575	0.745	0.304	0.473
58	2.68	0.33	0.00	−0.71	0.782	0.317	0.800	0.514	0.289
61	2.82	−0.01	0.00	−0.82	0.820	0.562	0.385	0.491	1.088

3.2.2. Application: 4-bit SHIFT register

The proposed prototypic 4-bit SHIFT register is a sequential logic circuit that has the ability to store and transfer information in the form of binary data (0 and 1). This logic device acts as a cascade of flip flops which loads the data present on the input and then shifts them to the right after every clock cycle (laser pulse in this case). The quest for a 4-bit spin-SHIFT register with Ni_4 is motivated by the prototypic spin-shift register proposed by

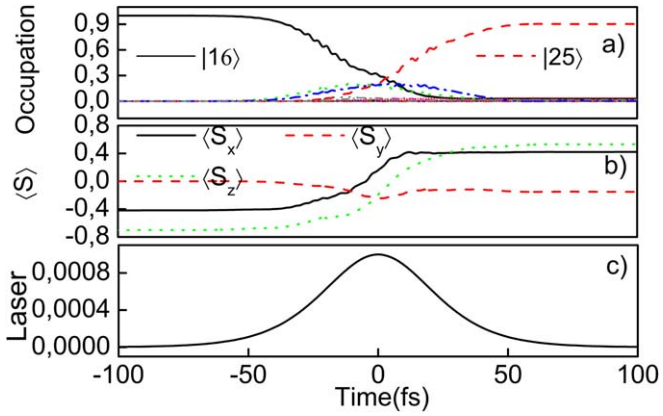

Figure 5. (a) Spin transfer scenario for Ni_4. The states $|16\rangle$ (solid black) and $|25\rangle$ (dashed red) are the initial and final state. (b) Time evolution of the expectation values of the the angular momentum components. (c) The envelope of the laser pulse.

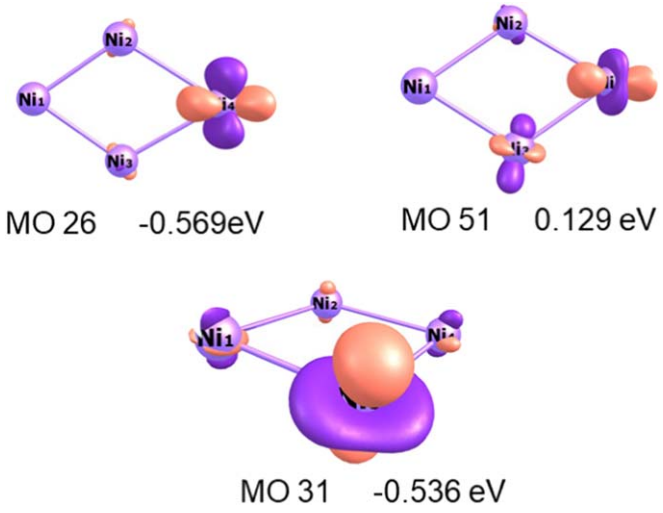

Figure 6. Some of the strongly localized, single electron, *d*-character molecular orbitals for Ni3 and Ni4 in the Ni_4 cluster. The multiplicity of the cluster for the HF step is a triplet. The isosurfaces of the molecular orbitals are dark violet and orange for positive and negative values, respectively.

Table 4. The optimized parameters of the laser pulses for the spin-transfer scenarios in Ni_4 discussed in this manuscript. Here, θ and ϕ denote the angles of the incidence in spherical coordinates, and γ is the angle between the polarization of the light and the optical plane. FWHM is the full width at half maximum of the laser pulse [10].

Transfer process	$\theta(^\circ)$	$\phi(^\circ)$	$\gamma(^\circ)$	Intensity(J s^{-1} m^{-2})	FWHM(fs)	Energy(eV)
Λ_1 (Ni1 → Ni2)	216.42	263.43	90.09	2.35	109	2.39
Λ_2 (Ni2 → Ni3)	0.00	64.05	25.69	0.59	300	2.67
Λ_3 (Ni4 → Ni3)	26.56	210.27	188.13	252.67	330.19	0.60
Λ_4 (Ni3 → Ni1)	100.86	15.84	275.01	0.15	421.69	3.15

Mahan [25]. The presence of an extra magnetic center allows us to increase the complexity by adding an extra bit to the 3-bit cyclic shift register. As discussed in the case of Co_3^+CO, we assign the binary 1 (else 0) to the atoms that have a significant localization of the spins. A linearly polarized laser pulse is used as a trigger to drive the transfer scenarios. In order to explain the laser-induced spin transfer scenarios more elaborately, we use the vector equation that is equivalent to a matrix equation of the form

$$L \cdot \mathbf{X} = \mathbf{A} \tag{5}$$

where L is a 4×4 matrix representing the laser pulse, $\mathbf{X}$ is a column vector with 4 entries and each entry represents the initial localization of the spin on any of the 4 magnetic center (Ni1, Ni2, Ni3, or Ni4) and lastly the

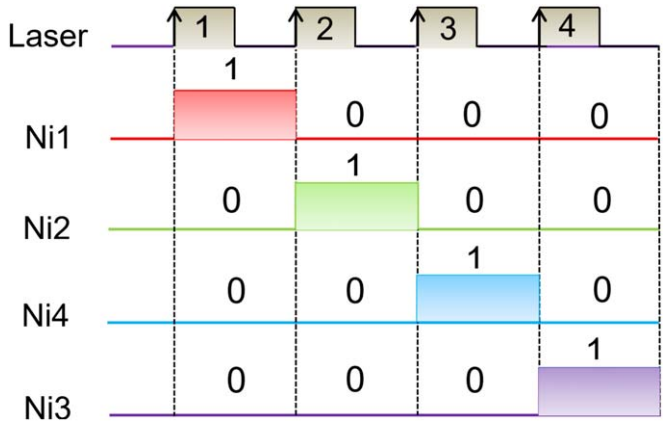

Figure 7. Schematic of information processing within the prototypic 4-bit spin-shift register. Note, after the end of each clock pulse (laser pulse in our case) the spin is transferred to the right side.

Table 5. A basic truth table for the 4-bit quantum-spin-shift register. The directional movement of the data in the register is to the right. The first column refers to the laser pulse (state), the second, third, fourth and fifth column refers to the localization of the spin on the centers, and the last column refers to the fidelity of the process.

Laser pulse	Ni1	Ni2	Ni4	Ni3	state	fidelity (f)
no laser	1	0	0	0	initial	100 %
Λ_1	0	1	0	0	achieved	86 %
Λ_2	0	0	1	0	achieved	97 %
Λ_3	0	0	0	1	achieved	80 %
Λ_4	1	0	0	0	achieved	91 %

column vector with **A** with 4 entries represent the target functionality. A more generalized form of the matrix equation is

$$\begin{pmatrix} l_{11} & l_{12} & l_{13} & l_{14} \\ l_{21} & l_{22} & l_{23} & l_{24} \\ l_{31} & l_{32} & l_{33} & l_{34} \\ l_{41} & l_{42} & l_{43} & l_{44} \end{pmatrix} \begin{pmatrix} x_1 \\ x_2 \\ x_3 \\ x_4 \end{pmatrix} = \begin{pmatrix} a_1 \\ a_2 \\ a_3 \\ a_4 \end{pmatrix} \tag{6}$$

The laser pulse is unique to every possible transfer scenario. With the appropriate choice of intermediate states and a different set of initial conditions, it is possible to obtain transfer scenarios between the same magnetic centers, however the optimization might yield a different set of laser parameters. The presence of the 4 active centers, allows us to control the localization of the spins between the centers. With respect to the localization of the spins on the Ni1, Ni2, Ni4 and Ni3 atoms (in the cyclic order as shown in figure 4) we represent the 4-bits as $|1000\rangle$, $|0100\rangle$, $|0010\rangle$, and $|0001\rangle$. A concise representation of the laser induced scenarios is $|1000\rangle \overset{\Lambda_1}{\rightarrow} |0100\rangle \overset{\Lambda_2}{\rightarrow} |0010\rangle \overset{\Lambda_3}{\rightarrow} |0001\rangle \overset{\Lambda_4}{\rightarrow} |1000\rangle$, where Λ_1, Λ_2, Λ_3 and Λ_4 are the different laser pulses triggering the shift. A pictorial representation of the spin-shift register mechanism is shown in figure 7. Each laser cycle basically represents a full clock cycle. We consider the spatially localized spins as the input and the output whereas the directions of the spin expectation values are not considered. Initially we set the proposed SHIFT register as $|1000\rangle$ which marks the initial step when the spin in localized on Ni1 (colored in red in figure 7) and the initial state for the process is $|51\rangle$. Then we apply the first laser (Λ_1) which transfers the electronic population to $|54\rangle$, which is Ni2, with a fidelity of 86%. This can be followed in the second row of table 5 where we can see the operation from $|1000\rangle$ to $|0100\rangle$ after the action of Λ_1. The next operation aims to transfer the spin from Ni2 to Ni4. Ideally the transfer of the electronic population should originate from the final state of the last cycle which $|54\rangle$. However, due to lack of addressable spin channels the best option is to find states that are energetically close and exhibit the same spin localization. For this operation we consider state $|58\rangle$, which is localized on Ni2. After the action of the second laser pulse (Λ_2) the electronic population gets transferred to Ni4 for which the final state is $|61\rangle$. The notation in the form of bits for this case is from $|0100\rangle$ to $|0010\rangle$. The fidelity of this process is (97%) shown in the third column of table 5. This process is shown in figure 7 by the clock cycles marked in green and blue. Similarly, to illustrate the operation $|0010\rangle \rightarrow |0001\rangle$ we choose $|14\rangle$ as the initial state (localized on Ni4) and $|16\rangle$ as the final state (for which the spin in localized on Ni3). This process takes place with the action of the third laser (Λ_3)with a

fidelity of 80%. In figure 7 this operation is marked with localization on Ni4 and Ni3 colored in blue and violet, and the transfer of the bits to the right is shown in table 5 in the fourth row. Lastly, to complete the entire cyclic process from $|0001\rangle$ to $|1000\rangle$ we transfer the spin from Ni3 to Ni1 with the action of a fourth laser (Λ_4). This process in shown in the fifth row of table 4. The initial and final states for the process are $|16\rangle$ and $|25\rangle$. Note that throughout the entire series of the processes the data can be reset to any initial state and the data will not lost as they will circle around. It is clear from figure 7 also that after each operation the information encoded in the spins, shifts to the right by 1 bit. We conclude that in our model of spin dynamics, the laser pulse drives the spin from one magnetic center to another, mimicking the logic operation of a conventional *Serial-In to Serial-Out* (SISO) shift register. The total transition time to complete the entire mechanism is less than 2 ps which is considerably fast.

As one can understand the electronic population will decay if the cycle is repeated in a loop. To keep this in check, one can think of spin pumping from the ground state. In reality, all the lost population would be accumulated in the ground state. So, once the active electronic population goes below a certain threshold limit, an additional laser pulse could be used to pump the ground state accumulated population to the intended initial state. Furthermore, it is also important to read out the information of states at each step after the clock cycle since the information states are coded as spin localization on the atoms. Thus, keeping in mind the experimental feasibility we propose read out scenarios that can be implemented on our molecule. In general, a magnetization sensor is extremely accurate within a very small spatial distance (a few Angstroms). There have been extensive investigations on sensors for magnetic nanomaterials. We can use the magnetization sensor to read out the magnetization in a very tiny region around a particular Co/Ni atom. This magnetic field will directly correspond to the spin of that Co/Ni atom. Note that just the magnitude of the magnetic field of the magnetization sensor would be sufficient to give us the output, the direction would not be necessary in this case. If now we set the magnetization sensor in a particular atom it will read out in a SISO fashion and if we set different magnetization sensors at the different Co/Ni atoms, then it will read out the outputs in a *Serial-In to Parallel-Out* SIPO fashion. The clock speed will be set according to the FWHM of the laser pulses. For example, in this case the second input will be loaded approximately 2×300 fs after the first clock tick as the first process will take approximately 2×109 fs to complete (109 fs is the FWHM of the first process). Similarly, the third input will be loaded 2×300 fs after the second clock tick (300 fs is the FWHM of the second process). The clock ticks according to the process (FWHM) can be easily programmed.

Table 5 shows the truth table for the prototypic 4-bit quantum-spin-shift register. The first row represents a situation in which no laser has been applied and the spin is initially localized on Ni1. The notation $|1000\rangle$ is used to describe such a scenario. This can be mapped to the situation of an ideal SHIFT-register where after the application of the first clock pulse, the output of the first bit is set to the value 1 while the output of the rest of the bits still remains 0. Now after the application of the laser pulses Λ_1, Λ_2, Λ_3 and Λ_4 the information stored in the register shifts to the right (see figure 7). The last column represents the efficiency for each process. Note, the efficiency of all the processes are above the minimum efficiency (60%) required for any logic operation in modern transistor-transistor logic (TTL) circuits in which typically a voltage between 0.0 and 1.5 V represents the 0 bit (30% efficiency), while a voltage between 3.0 and 5.0 V stands for the 1 bit (a minimum of 60% efficiency) [7]. We believe that the proposed analysis of the 4-bit quantum-spin-SHIFT register serves as a useful road map for future spin-memory devices synthesized with real magnetic clusters. Thus, manipulating the spins between the magnetic centers, the register can be configured to respond to certain sequential logic operations that require some form of temporary storage.

4. Conclusions

We summarize our findings as following:

In Co_3^+CO: (i) Based on a cycle of spin-transfer scenarios we develop a prototypic cyclic 3-bit spin-SHIFT register with an operational time of 2 ps approximately. The efficiency of all spin manipulation scenarios are at least 69%. (ii) To physically understand the transferability of three component transfer scenarios, the analysis of the electronic spectra for the related initial and final states is exhibited. (iii) A detailed inspection shows that a reverse cycle of the second spin transfer scenario (Co2 $\longrightarrow$Co3) is blocked due to its irreversibility. This can be attributed to the cooperative effects of too many involved intermediate states, their large expanded energy region, and their noticeable occupations during the propagation.

In Ni_4: (i) Exploiting the laser-driven spin-transfer scenarios between the active centers we develop a prototypic 4-bit spin-SHIFT register that has the ability to store and process information encoded in the spins. (ii) The total operation time of proposed shift-register is 2 ps approximately. (iii) The present study serves as a proof-of-principles of the logic element arising from structures with four magnetic centers.

The results obtained in this manuscript provide a promising approach for realizing controllable ultrafast magnetic dynamics in realistic multinuclear magnetic molecular structures and demonstrate their great potential in spin-logic device design and future nanospintronic applications.

Acknowledgments

We acknowledge financial support from the National Natural Science Foundation of China (Grants No. 11504223 and No. 11872309), Natural Science Basic Research Plan in Shaanxi Province (No. 2017JM1033), and the Fundamental Research Funds for the Central Universities (Grant No. GK201903015). W.J. and D.C. contributed equally to this manuscript.

Data availability statement

All data that support the findings of this study are included within the article (and any supplementary files).

Appendix A: Additional computational details

A.1. Symmetry-adapted cluster configuration-interaction

In SAC-CI the ground state is

$$|\gamma_g\rangle = \left(1 + \sum_I c_I S_I + \frac{1}{2}\sum_{I,J} c_I c_J S_I S_J + \ldots\right)|\Phi_0\rangle. \tag{A.1}$$

In the above equation $|\Phi_0\rangle$ is the Hartree–Fock many-body wavefunction, S_I, S_J are the symmetry-adapted excitation operators (single, double or higher excitations) and c_I are the expansion coefficients. The single-excitation operators are

$$S_I = S_i^a = \frac{1}{\sqrt{2}}(a_{a\alpha}^{\dagger} a_{i\alpha} + a_{a\beta}^{\dagger} a_{i\beta}). \tag{A.2}$$

Operating on $|\Phi_0\rangle$ with S_I means destroying an electron in the molecular orbital i and creating one in the molecular orbital a. This is extended for the α(spin-up)- and β(spin-down)-electrons. Finally the excited states are determined via the cluster expansion of the SAC-CI wavefunction [48],

$$\begin{aligned}|\gamma_e\rangle = &\left(\sum_K d_K R_K + \sum_{K,I} d_K c_I R_K S_I + \ldots\right)|\Phi_0\rangle \\ &- \sum_K d_K S_{gK}|\gamma_g\rangle,\end{aligned} \tag{A.3}$$

where $S_{gK} = \langle\gamma_g|R_K|\gamma_g\rangle$. d_K are the normalization coefficients and R_K represents the excitation operator of the excited system.

Appendix B: Optical spectra

When discussing the functionalization of a logic element it is interesting to also discuss the optical spectra (OS) to understand the transferablity between the initial and final states and some of the intermediate states mediating a major proportion of the population.

We analyze the optical spectra of the three interesting states (i.e., states $|1\rangle$, $|35\rangle$, and $|37\rangle$) of Co, as shown in figure 8. The abscissa of each subfigure denotes energy difference between each specified electronic state and the rest 119 states whereas the ordinate shows the oscillator strength. The latter basically represents the intensity of the peaks (in arbitrary units) and is calculated as following:

$$I_{|i\rangle\to|f\rangle} = \Gamma(E_{|f\rangle} - E_{|i\rangle})|D_{|i\rangle\to|f\rangle}|^2 \tag{B.1}$$

where $E_{|i\rangle}$ and $E_{|f\rangle}$ are the energies of the states $|i\rangle$ and $|f\rangle$, Γ denotes the artificial broadening of the peaks and $|D_{|i\rangle\to|f\rangle}|$ gives the electric-dipole transition matrix elements between the states. The zero points (marked with solid black square points) in figure 8 refer to different energy positions, namely, from down to up they represent 0 (the ground state), 1.205 (state $|35\rangle$), and 1.272 eV (state $|37\rangle$), respectively. Note here that the electronic states can be identified from the absolute energies read from the abscissa of the bottom panel (i.e., vertically the three different energy difference values correspond to the same state). The peaks with the negative energy values in the upper two panels indicate that the transitions occur between the specified states and their lower states. Clearly,

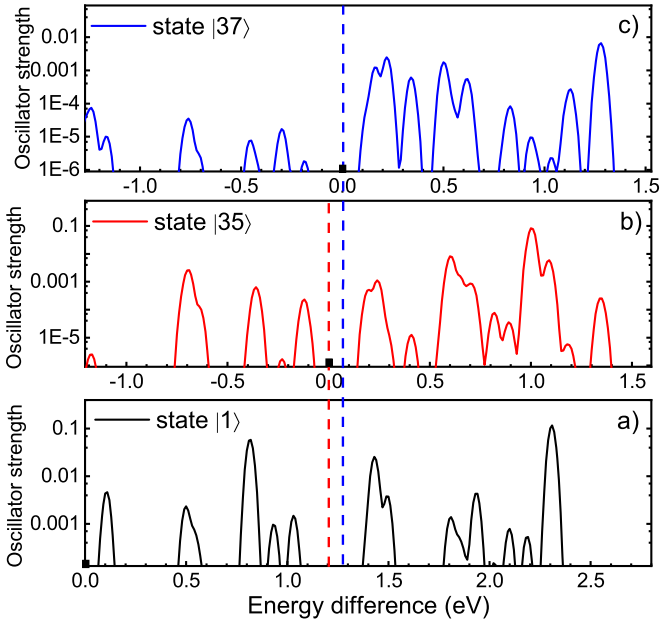

Figure 8. (a), (b) and (c) are the optical spectra of states $|1\rangle$, $|35\rangle$, and $|37\rangle$, respectively. The spectra are calculated from the oscillator strengths in arbitrary units with a Gaussian broadening of 0.015 eV. The dashed red and dash-dotted blue lines represent the energy positions of state $|35\rangle$ and $|37\rangle$ with respect to the ground-state spectra.

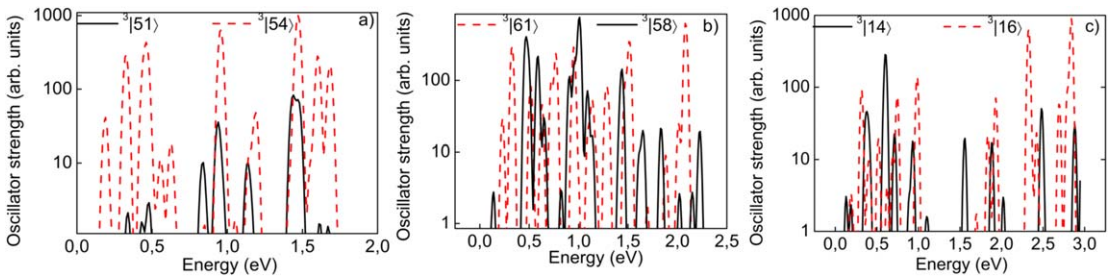

Figure 9. Optical spectra of the initial states and final for the spin transfer scenarios in Ni_4. (a) Ni1 ⟶Ni2, (b)Ni2 ⟶Ni4 and (c) Ni4 ⟶Ni3 (details of spin dynamics scenarios are discussed in another article [10]).

since no peaks with transition magnitudes above 10^{-4} appear between any two of the three states, the direct transitions of them are regarded to be forbidden. However, due to the participation of a number of common states (e.g., the states with energies around 0.5 and 0.8 eV, and the states with energies lying in the regions of 1.4–1.5 eV and 1.8–2.3 eV) that have similar transition peaks at the same absolute energy positions in the spectra, their indirect transitions are allowed. Therefore, the transferability of the three Λ-process based spin-transfer scenarios becomes possible.

Figure 9(a) refers to the OS of the initial ($|51\rangle$) and final state ($|54\rangle$) for the Ni1 → Ni2 process. The presence of multiple peaks is a signature of transitions between many intermediate states. However, an acute comparison of the differences between the states allows us to trace the transitions exactly. Note, we present the absolute energy difference between the states in the abscissa. The overlap of the peaks of the solid black line ($|51\rangle$) and the dashed-red line ($|54\rangle$) confirms the transitions between common intermediate states. To elaborate it better, we consider the peak positioned at 1.00 eV marked by the solid black line. It refers to the transition $|51\rangle \longrightarrow |24\rangle$ which corresponds to an energy difference of $\Delta E_{|51\rangle \longrightarrow |24\rangle} = 0.97$ eV. Now, comparing it to the peak denoted by the red-dashed lines at 1.013 ev we see it is shifted by 0.013 eV. This is more or less comparable to the energy difference between $|51\rangle$ and $|54\rangle$ i.e., $\Delta E_{|51\rangle \longrightarrow |54\rangle} = 0.013$ eV. Similarly the transitions corresponding to other peak positions can be traced but this goes beyond the scope of this manuscript.

Similarly, figure 9(b) represents the optical spectra of the initial ($|58\rangle$) and final ($|61\rangle$). The isolated peak denoted by the solid black line positioned at 1.4 eV is a result of the transition between $|58\rangle \longrightarrow |22\rangle$ and the corresponding transition energy is $\Delta E_{|58\rangle \longrightarrow |22\rangle} = 1.4$ eV. Comparing it with the partially overlapped peak

represented by the dashed-red line at 1.5 eV, we see it is shifted to the left by approximately 0.1 eV. This corresponds to the transition between $|61\rangle \longrightarrow |22\rangle$ and the corresponding transition energy is $\Delta E_{|61\rangle \longrightarrow |24\rangle} = 1.5$ eV. The absolute energy difference between the $|58\rangle$ and $|61\rangle$ is nearly 0.1 eV. This corresponds to the shift in the position of the peaks.

Figure 9(c) represents the optical spectra for states $|14\rangle$ (solid black line) and $|16\rangle$ (dashed red line). In this case we consider an peak marked with the solid black line and positioned at 2.5 eV. This corresponds to the optical transition between the states $|14\rangle \longrightarrow |75\rangle$ having an absolute energy difference of $\Delta E_{|14\rangle \longrightarrow |75\rangle} = 2.5$ eV. Now the transition energy for $|16\rangle \longrightarrow |75\rangle$ is $\Delta E_{|16\rangle \longrightarrow |75\rangle} = 2.31$ eV. Thus an absolute energy difference of approximately 0.19 eV between the position of these two peaks is nearly equal to the energy difference $\Delta E_{|16\rangle \longrightarrow |14\rangle} = 0.19$ eV. Thus, for both the transitions $|75\rangle$ is common and the corresponding peaks are shifted by an energy that corresponds to the transition energy between the initial and final state.

ORCID iDs

G Lefkidis https://orcid.org/0000-0003-1181-3704
D Chaudhuri https://orcid.org/0000-0002-8914-3053
C Li https://orcid.org/0000-0002-0901-0294

References

[1] Maekawa S and Shinjo T 2002 *Spin Dependent Transport in Magnetic Nanostructures* (Taylor & Francis)
[2] Parkin S, Jiang X, Kaiser C, Panchula A, Roche K and Samant M 2003 *Proc. IEEE* **91** 661
[3] Behin-Aein B, Datta D, Salahuddin S and Datta S 2010 *Nature Nanotech.* **5** 266
[4] Khajetoorians A A, Wiebe J, Chilian B and Wiesendanger R 2011 *Science* **332** 1062
[5] Žutić I and Fuhrer M 2005 *Nat. Phys.* **1** 85
[6] Wolf S A, Awschalom D D, Buhrman R A, Daughton J M, von Molnár S, Roukes M L, Chtchelkanova A Y and Treger D M 2001 *Science* **294** 1488
[7] Hübner W, Kersten S and Lefkidis G 2009 *Phys. Rev. B* **79** 184431
[8] Žutić I, Fabian J and Das Sarma S 2004 *Rev. Mod. Phys.* **76** 323
[9] Mummaneni C B, Liu J, Lefkidis G and Hübner W 2022 *J. Phys. Chem. Lett.* **13** 2479
[10] Chaudhuri D, Lefkidis G and Hübner W 2017 *Phys. Rev. B* **96** 184413
[11] Hofherr M *et al* 2020 *Sci. Adv.* **6**
[12] Chen J, Bovensiepen U, Eschenlohr A, Müller T, Elliott P, Gross E K U, Dewhurst J K and Sharma S 2019 *Phys. Rev. Lett.* **122** 067202
[13] Maekawa S 2004 *J. Magn. Magn. Mater.* **272-276** E1459
[14] Parkin S 2008 *IEEE/SEMI Advanced Semiconductor Manufacturing Conference* 221–221
[15] Parkin S, Jiang X, Kaiser C, Panchula A, Roche K and Samant M 2003 *Proceedings of the IEEE* 91 661
[16] Renaud N and Joachim C 2008 *Phys. Rev. A* **78** 062316
[17] Beaurepaire E, Merle J-C, Daunois A and Bigot J-Y 1996 *Phys. Rev. Lett.* **76** 4250
[18] Zhang G P and Hübner W 2000 *Phys. Rev. Lett.* **85** 3025
[19] Hübner W and Zhang G P 1998 *Phys. Rev. B* **58** R5920
[20] Bogani L 2014 *Experiments on Molecular Magnets for Molecular Spintronics* (Springer) 331 chap. 8
[21] Joachim C 2002 *Nanotechnology* **13** R1
[22] van der Molen S J and Liljeroth P 2010 *J. Phys. Condens. Matter* **22** 133001
[23] Sanvito S 2011 *Chem. Soc. Rev.* **40** 3336
[24] Heinrich A and Loth S 2011 *Science* **332** 1039
[25] Mahan G D 2009 *Phys. Rev. Lett.* **102** 016801
[26] Lefkidis G, Jin W, Liu J, Dutta D and Hübner W 2020 *J. Phys. Chem. Lett.* **11** 2592
[27] Baskin I, Zaitsev S, Lipson D, Gilad R, Keren K, Ben-Yoseph G and Sivan U 2006 *Phys. Rev. Lett.* **97** 208103
[28] Lengwenus A, Kruse J, Schlosser M, Tichelmann S and Birkl G 2010 *Phys. Rev. Lett.* **105** 170502
[29] Xiang H, Lefkidis G and Hübner W 2013 *J. Supercond. Nov. Magn.* **26** 2001
[30] Li C, Jin W, Xiang H, Lefkidis G and Hübner W 2011 *Phys. Rev. B* **84** 054415
[31] Jin W, Li C, Lefkidis G and Hübner W 2014 *Phys. Rev. B* **89** 024419
[32] Chaudhuri D, Jin W, Lefkidis G and Hübner W 2015 *J. Chem. Phys.* **143** 174303
[33] Li C, Liu J, Lefkidis G and Hübner W 2017 *Phys. Chem. Chem. Phys.* **19** 673
[34] Li C, Zhang S, Jin W, Lefkidis G and Hübner W 2014 *Phys. Rev. B* **89** 184404
[35] Pavlyukh Y, Rentschler E, Elmers H-J, Hübner W and Lefkidis G 2018 *Phys. Rev. B* **97** 214408
[36] Barhoumi M, Liu J, Lefkidis G, Hübner W and Jin W 2023 *J. Chem. Phys.* **159** 084304
[37] Corbett B, Bower C, Fecioru A, Mooney M, Gubbins M and Justice J 2013 *Semicond. Sci. Technol.* **28** 094001
[38] He L and Li M 2014 *Opt. Lett.* **39** 2553
[39] Becker H, Krückel C J, Van Thourhout D and Heck M J R 2019 *2019 Conference on Lasers and Electro-Optics Europe & European Quantum Electronics Conference (CLEO/Europe-EQEC)* 1–1
[40] Becker H, Krückel C J, Van Thourhout D and Heck M J R 2020 *IEEE J. Sel. Top.* **26** 1
[41] Steil D *et al* 2020 *Phys. Rev. Research* **2** 023199
[42] Shokeen V, Sanchez Piaia M, Bigot J-Y, Müller T, Elliott P, Dewhurst J K, Sharma S and Gross E K U 2017 *Phys. Rev. Lett.* **119** 107203
[43] Berritta M, Mondal R, Carva K and Oppeneer P M 2016 *Phys. Rev. Lett.* **117** 137203
[44] Halilov S V, Eschrig H, Perlov A Y and Oppeneer P M 1998 *Phys. Rev. B* **58** 293
[45] Chaudhuri D, Xiang H P, Lefkidis G and Hübner W 2014 *Phys. Rev. B* **90** 245113
[46] Wadt W R and Hay P J 1985 *J. Chem. Phys.* **82** 284

[47] Hay P J and Wadt W R 1985 *J. Chem. Phys.* **82** 299
[48] Nakatsuji H 1979 *Chem. Phys. Lett.* **67** 329
[49] Krylov A I 2001 *Chem. Phys. Lett.* **338** 375
[50] Meissner L and Bartlett R J 1991 *J. Chem. Phys.* **94** 6670
[51] Nooijen M, Shamasundar K R and Mukherjee D 2005 *Mol. Phys.* **103** 2277
[52] Stanton J F 1994 *J. Chem. Phys.* **101** 8928
[53] Szabo A and Ostlund N S 1996 *Modern quantum chemistry : introduction to Advanced Electronic Structure Theory.* (Dover publications)
[54] Koseki S, Schmidt M W and Gordon M S 1998 *J. Phys. Chem. A* **102** 10430
[55] Cash J R and Karp A H 1990 *ACM Trans. Math. Softw.* **16** 201
[56] Hartenstein T, Li C, Lefkidis G and Hübner W 2008 *J. Phys. D: Appl. Phys* **41** 164006
[57] Li C, Zhang S, Jin W, Lefkidis G and Hübner W 2014 *Phys. Rev. B* **89** 184404
[58] Xiao L and Wang L 2004 *J, Phys. Chem. A* **108** 8605
[59] Kolehmainen J, Häkkinen H and Manninen M 1997 *Z Phys D—Atoms, Molecules and Clusters* **40** 306–9
[60] Jakob P, Anhut K, Schnur S and Groß A 2008 *Phys. Rev. Lett.* **101** 206101
[61] Mannini M *et al* 2009a *Nature Mater 8, 194-197 (2009)* **8** 194
[62] Mannini M *et al* 2009 *Adv. Mater.* **21** 167
[63] Pal G, Lefkidis G and Hübner W 2009 *J. Phys. Chem. A* **113** 12071
[64] Pal G, Lefkidis G, Schneider H C and Hübner W 2010 *J. of Chem. Phys.* **133** 154309
[65] Jin W, Becherer M, Bellaire D, Lefkidis G, Gerhards M and Hübner W 2014 *Phys. Rev. B* **89** 144409
[66] Li C, Hartenstein T, Lefkidis G and Hübner W 2009 *Phys. Rev. B* **79** 180413
[67] Fielicke A, von Helden G, Meijer G, Pedersen D B, Simard B and Rayner D M 2006 *J. Chem. Phys.* **124** 194305
[68] Jin W, Chaudhuri D, Li C, Lefkidis G and Hübner W 2017 *J. Supercond. Nov. Magn.* **30** 801
[69] Li C, Zhang S, Jin W, Lefkidis G and Hübner W 2014c *Phys. Rev. B* **89** 184404
[70] Zhang G P, Lefkidis G, Hübner W and Bai Y 2012 *J. Appl. Phys.* **111** 07C508
[71] DiVincenzo D P 2000 *Fortschr. Phys* **48** 771
[72] Bogani L and Wernsdorfer W 2008 *Nat. Mater.* **7** 179
[73] Ardavan A, Rival O, Morton J J L, Blundell S J, Tyryshkin A M, Timco G A and Winpenny R E P 2007 *Phys. Rev. Lett.* **98** 057201
[74] Xiang H, Lefkidis G and Hübner W 2012 *Phys. Rev. B* **86** 134402
[75] Rafiquzzaman M 2005 *Fundamentals of Digital Logic and Microcomputuer Design* (Wiley)
[76] Kirchner N, van Slageren J, Tsukerblat B, Waldmann O and Dressel M 2008 *Phys. Rev. B* **78** 094426
[77] Petkov P St, Vayssilov G N, Krüger S and Rösch N 2006 *Phys. Chem. Chem. Phys.* **8** 1282
[78] Li C, Zhang S, Jin W, Lefkidis G and Hübner W 2014d *Phys. Rev. B* **89** 184404
[79] Li C, Liu J, Zhang S, Lefkidis G and Hübner W 2015 *Carbon* **87** 153
[80] Barolo C *et al* 2006 *Inorg. Chem.* **45** 4642
[81] Pritchard B P, Altarawy D, Didier B, Gibson T D and Windus T L 2019 *J. Chem. Inf. Model.* **59** 4814
[82] Schuchardt K L, Didier B T, Elsethagen T, Sun L, Gurumoorthi V, Chase J, Li J and Windus T L 2007 *J. Chem. Inf. Model.* **47** 1045